Reaction Mechanism of Deoxyribonucleotidase: A Theoretical Study

ARTICLE *in* THE JOURNAL OF PHYSICAL CHEMISTRY B · NOVEMBER 2005

Impact Factor: 3.3 · DOI: 10.1021/jp0546150 · Source: PubMed

Reaction Mechanism of Deoxyribonucleotidase: A Theoretical Study

Fahmi Himo,*,† Jing-Dong Guo,† Agnes Rinaldo-Matthis,‡ and Pär Nordlund‡

Theoretical Chemistry, Department of Biotechnology, Royal Institute of Technology, ALBANOVA, SE−106 91 Stockholm, Sweden and Department of Medicinal Biochemistry and Biophysics, Karolinska Institutet, SE-171 77 Stockholm, Sweden

Received: August 16, 2005

The reaction mechanism of human deoxyribonucleotidase (dN) is studied using high-level quantum-chemical methods. dN catalyzes the dephosphorylation of deoxyribonucleoside monophosphates (dNMPs) to their nucleoside form in human cells. Large quantum models are employed (99 atoms) based on a recent X-ray crystal structure [Rinaldo-Matthis et al. *Nat. Struct. Biol.* **2002**, *9*, 779]. The calculations support the proposed mechanism in which Asp41 performs a nucleophilic attack on the phosphate to form a phospho−enzyme intermediate. Asp43 acts in the first step as an acid, protonating the leaving nucleoside, and in the second step as a base, deprotonating the lytic water. No pentacoordinated intermediates could be located.

I. Introduction

Deoxynucleotidases (dNs) catalyze the dephosphorylation of deoxyribonucleotide monophosphates (dNMPs) to their nucleoside form in human cells (Scheme 1). They are involved in the regulation of deoxyribonucleotide pools, functioning to keep a balance of the dNTP precursors used for DNA replication in the cell.[1] Deoxynucleotidases together with nucleoside kinases constitute a so-called substrate cycle,[2] where thymidine kinase-1 and the cytosolic deoxyribonucleotidase (cdN) are active in the cytosol whereas thymidine kinase-2 and the mitochondrial deoxyribonucleotidase (mdN) are active in the mitochondria.[3] The enzymes regulating the substrate cycles are important medically. Many antiviral and anticancer nucleoside analogues used therapeutically rely on the activity of the substrate cycle when nucleoside analogues need to be phosphorylated by nucleoside kinases in order to carry out their toxic effect as chain terminators of DNA polymerization. dNs dephosphorylate dNMPs and thereby reduce the effect of the delivered drug. Thus, it has been suggested that inhibition of dNs would raise the effect of the delivered drug.[4,5]

Human mdN, the subject for this study, is a dimeric protein that requires Mg^{2+} for catalysis. The isomeric cytosolic protein (52% sequence identical to mdN) and mdN show similar substrate specificity, where the pyrimidine nucleotides dUMP5′ and dTMP5′ are preferred.

The X-ray crystal structures have been solved for both the cytosolic and the mitochondrial forms, revealing similar structures of two domains, a small 4-helix bundle, and an α/β fold.[6] The active site is situated in a cleft between the two domains and consists of four Asp residues, an Mg^{2+}, a lysine, and a threonine (See Figure 1).

The structure of the dNs can be grouped together with the haloacid dehalogenase (HAD) superfamily despite the fact that there is no overall sequence homology but in agreement with the three conserved motifs (DXD, S/T, and KXXDD). The HAD superfamily has members such as phosphoserine phosphatase,[7] haloacid dehalogenase,[8] Ca-ATPase P-subunit,[9] and β-phosphoglucomutase (β-PGM),[10] all with diverse functions but similar α/β fold and architecture of the active site. All HAD proteins use a phosphorylated Asp to perform their catalytic function. Allegrini et al. suggested that the soluble nucleotidases, including the dNs, form a phospho−enzyme intermediate during the reaction.[11]

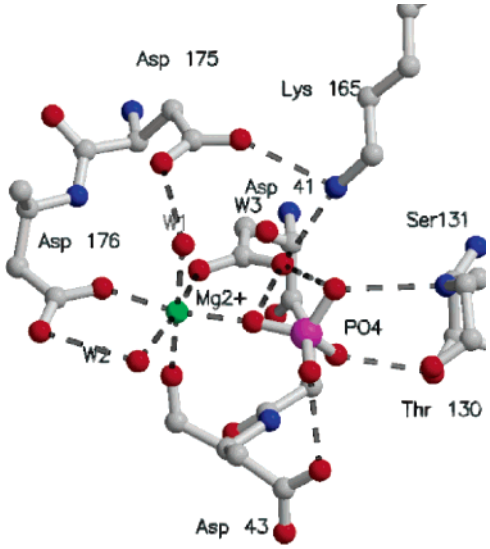

Figure 1. X-ray crystal structure of the active site of mdN with a phosphate group bound.[6]

Human mdN has been solved in complex with different inhibitors and transition-state analogues.[6,12] One of the most interesting structures mechanistically is the mdN in complex with BeF_3^-, which contains a water molecule at a suitable position for an in-line attack of the Asp-phospho group.

The following mechanism has been suggested for reaction of mdN (see Scheme 2).[6] The reaction starts with binding of the substrate. The negatively charged phosphate part of the nucleotide ($R-PO_4^{2-}$) coordinates to the Mg^{2+} ion and the positively charged Lys165. Next, Asp41 performs a nucleophilic attack on the phosphorus atom of the nucleotide with subsequent formation of a hypothetical pentavalent phospho−enzyme intermediate. Formation of a pentavalent intermediate is sup-

† Royal Institute of Technology.
‡ Karolinska Institutet.

10.1021/jp0546150 CCC: $30.25
Published on Web 10/04/2005

SCHEME 1. Reaction Catalyzed by Deoxynucleotidases

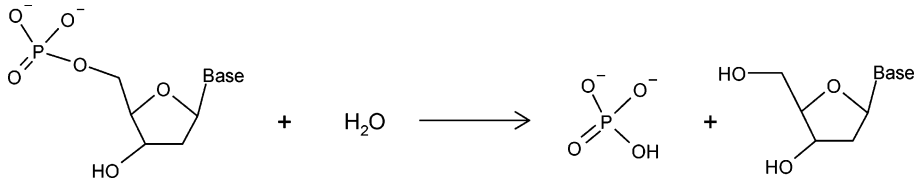

SCHEME 2. Proposed Reaction Mechanism for Deoxyribonucleotidase[6]

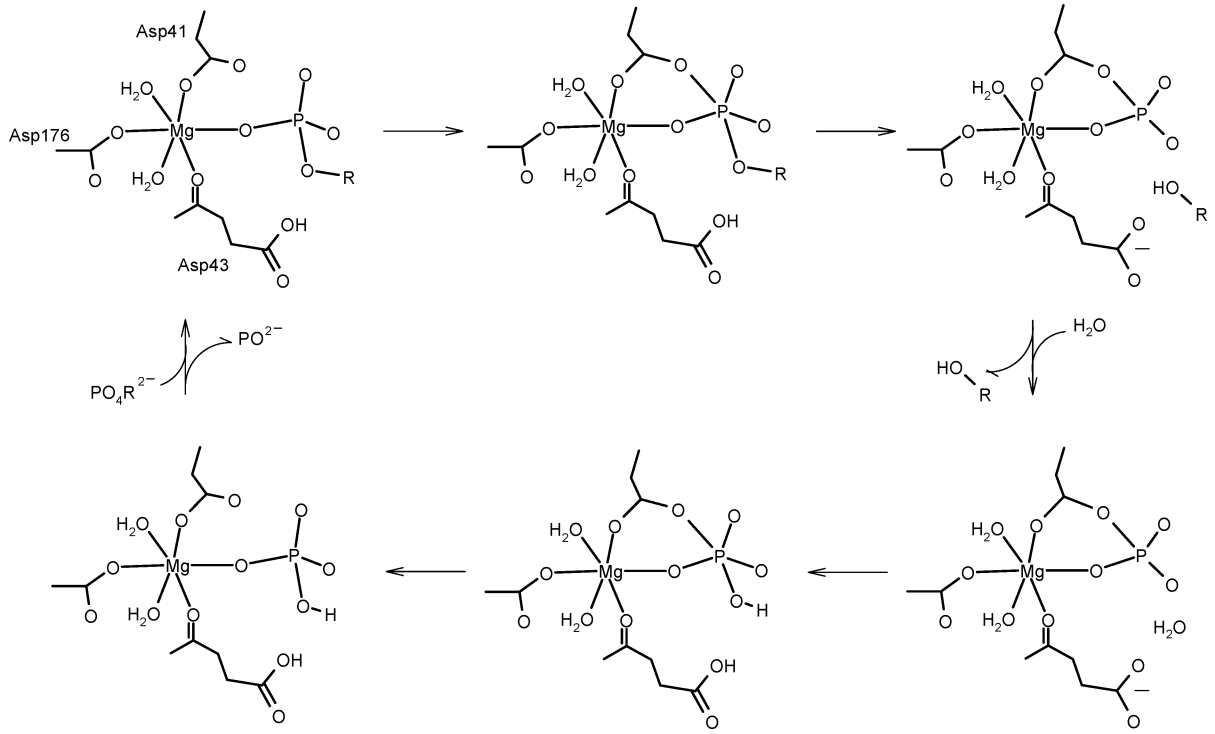

ported by the structure of β-PGM,[13] where a pentacoordinated phosphate intermediate was trapped in the crystal structure. The next step involves Asp43, which acts as an acid, protonating the leaving group. A water molecule now replaces the nucleoside product, and Asp43 now acts as a base in this step to activate the water, which attacks the phosphate to form a pentavalent intermediate structure. The phospho−enzyme bond is then broken to regenerate the enzyme.

In the present paper we investigated this mechanism employing a quite large quantum chemical model, consisting of up to 99 atoms, based on the crystal structure.[6] We use the hybrid density functional theory (DFT) method B3LYP, which has been widely used to study this kind of reactions in recent years.

II. Computational Details

All geometries and energies presented in the present study are computed using the B3LYP[14] density functional theory method as implemented in the Gaussian98 program package.[15] Geometry optimizations were performed using the LANL2DZ basis set. On the basis of these geometries, single-point calculations with the larger basis set 6-311+G(2d,2p) were done to obtain more accurate energies. Solvation energies were added as single-point calculations using the conductor-like solvation model COSMO[16] at the B3LYP/LANL2DZ level as implemented in the Gaussian03 program package.[17] In this model a cavity around the system is surrounded by a polarizable dielectric continuum. Two sets of COSMO calculations were performed, one with $\epsilon = 4$ to model protein surrounding and one with $\epsilon = 80$ to model water surrounding.

III. Chemical Models

In the initial phase of this study we used a relatively small model of the active site of deoxynucleotidase consisting of ca.

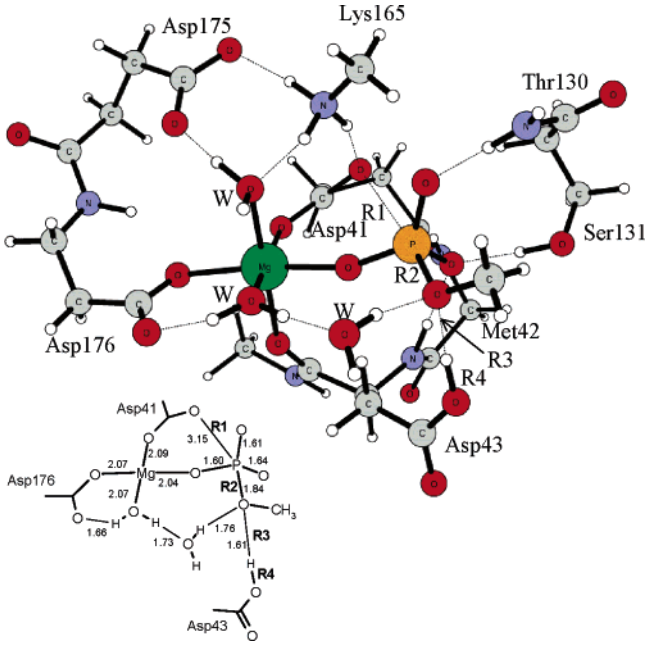

Figure 2. Model of the deoxynucleotidase active site used in the present calculations. Inserted is a schematic figure with important distances in Angstroms, as obtained from the geometry optimization procedure.

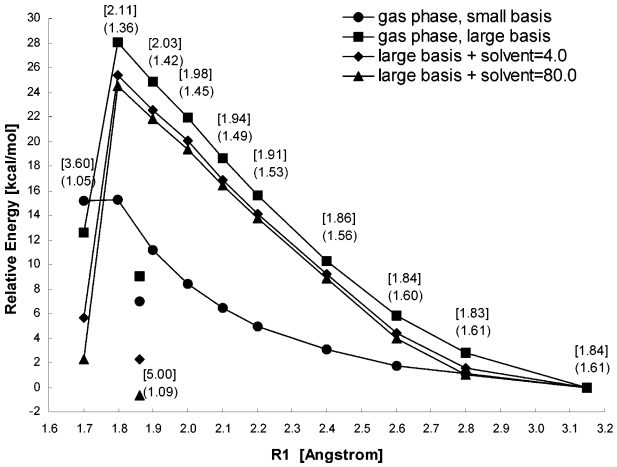

Figure 3. Potential-energy curves for the dephosphorylation step. Isolated points represent the energy of the product species, which has an unconstrained R1 distance of 1.86 Å. For each point, the values of R2 and R3 are given in Angstroms in brackets and parentheses, respectively.

50 atoms. However, this model was unstable under geometry optimization as various parts moved to form more favorable hydrogen bonds. To avoid having many centers kept frozen in order to get a reasonable agreement with the X-ray structure, we increased the model size gradually and finally arrived at a geometrically very stable model consisting of 99 atoms, as displayed in Figure 2. In this model the following parts are included: The Mg^{2+} ion with its ligands Asp176, Asp41, Asp43, and two water molecules. Interestingly, Asp43 is coordinated to Mg by its carbonyl oxygen and not its carboxylate, which will be involved in the proton-transfer events. The backbone atoms of Met42 were included for two reasons. First, they form a bridge between the Mg ligands Asp41 and Asp43. Second, the peptide bonds of this residue form hydrogen bonds to the substrate oxygens and are thus needed to stabilize the negative charge of the substrate. For the same reason, parts of Thr130 and Ser131 were included (as shown in Figure 2). A relatively small model of the positively charged side chain of Lys165 was included ($CH_3NH_3^+$) as it forms three hydrogen bonds to the different oxygens and contributes to the overall stability of the model. Asp175 was included in its entirety. The substrate was modeled using a $PO_4CH_3^{2-}$ moiety (see Figure 2). This is adequate and resembles the properties of the P−O and H−O bonds of the nucleotide quite well. Finally, an ordered water molecule that forms a hydrogen bond to the substrate was also included.

With all these parts the total charge of this model becomes −2, which is the charge of the phosphate part of the substrate. No atoms needed to be fixed in order to get a good agreement with the crystal structure. Interestingly, most of the residues included in this model correspond to residues that are conserved among the dNs.

IV. Reaction Mechanism

a. Dephosphorylation. The first step in the proposed mechanism (Scheme 2) is formation of the asparatyl−phosphate adduct intermediate. In the optimized geometry of the reactant (Figure 2) the distance between O^{γ} of Asp41 and the phosphor center (hereafter called R1, see definitions in Figure 2) is 3.15 Å, which is in good agreement with the 3.0 Å found in the X-ray structure. We choose R1 as the reaction coordinate for the first step, the attack of Asp41 on the phosphate. R1 is fixed at different values, and all other degrees of freedom are optimized in a linear transit (LT) scheme. The results of this procedure are shown in Figure 3. In the figure we give the energy using both the small basis set, LANL2DZ, and the large basis set, 6-311+G(2d,2p). The energy is also given including solvation effects with both $\epsilon = 4$ and 80.

As O^{γ} approaches P, i.e., R1 gets smaller, we see that the trans P−O bond distance (called R2) increases slowly and the carboxylic proton of Asp43 moves toward the leaving oxygen (R3 decreases and R4 increases). The energy increases monotonically until R1 = 1.8 Å. After that, a small change in R1 causes a big change in the energy because now the proton of Asp43 suddenly moves fully to the nucleoside, which then dissociates completely from the phosphate. It is very important to note here that the fully optimized product of this reaction step (with unconstrained R1) has an R1 value of 1.86 Å, i.e., larger than R1 = 1.80 Å, the distance shorter than which the nucleoside dissociates (see Figure 4). This is a typical hysteresis phenomenon which originates from the fact that the chosen reaction coordinate (R1) does not fully represent the chemistry

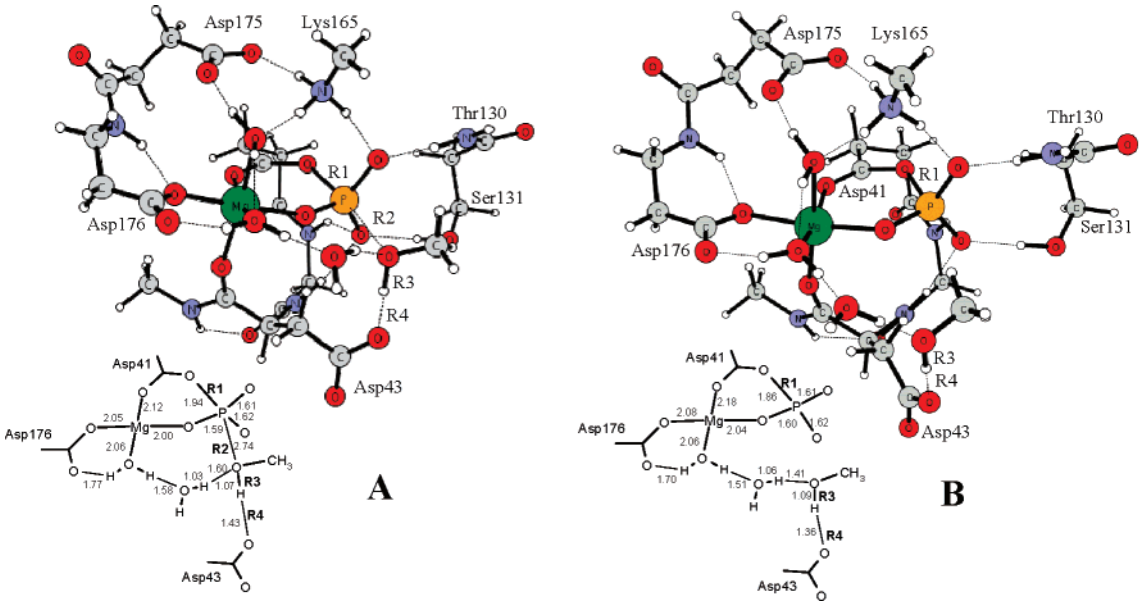

Figure 4. Optimized structures of the transition state (A) and product (B) of the nucleoside dissociation step.

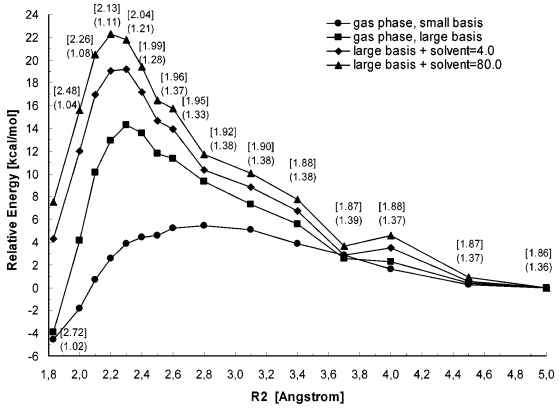

Figure 5. Potential-energy surface for the hydrolysis step. For each point the values of R1 and R4 are given in Angstroms in brackets and parentheses, respectively.

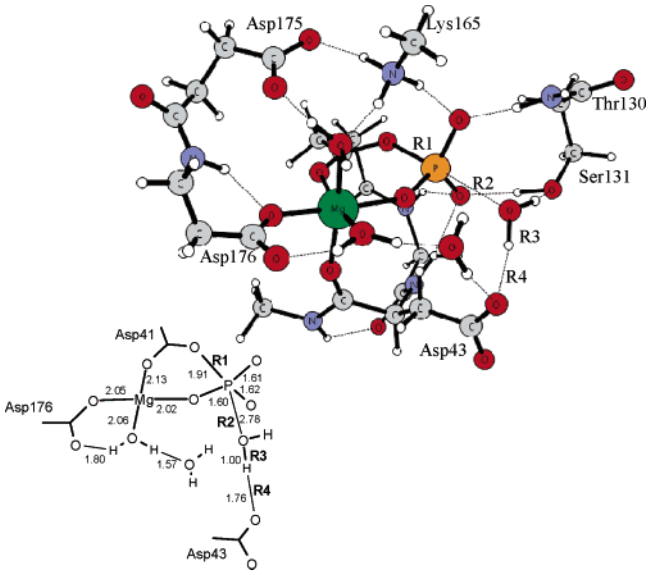

Figure 6. Optimized transition-state structure for the hydrolysis step.

that takes place. To solve this problem one can vary some other degree(s) of freedom independently (for example, R2 and R3) and evaluate the energy on a grid. This requires a large number of geometry optimization calculations and is very demanding to perform with a quantum-chemical model of this size. A better approach is, however, to find the exact transition state for the reaction.

In the present study we managed to optimize the exact unconstrained transition state for this reaction step (structure shown in Figure 4). The R1 and R2 distances at the transition state are 1.94 and 2.75 Å, respectively, to be compared to 1.80 and 2.11 Å obtained for the highest point of the LT procedure. The barrier is found to be 16.6 kcal/mol in the gas phase and 11.1 kcal/mol with $\epsilon = 4$, which is considerably lower than the LT results presented above (>24 kcal/mol at R1 = 1.8 Å). The dissociation reaction step is quite endothermic (+9.0 kcal/mol) in the gas phase, but the solvation effects make the step slightly exothermic instead (−0.7 kcal/mol using $\epsilon = 4$). The large difference between the gas phase and solvation results can be understood if we note that Asp43, which is changing its charge state from neutral to anionic during the reaction step, is located at the edge of the quantum-chemical model. This will result in different solvation energies between reactant and product.

We made several attempts to locate a pentacoordinated intermediate structure such as the one proposed in Scheme 2 without any success. We have of course not ruled out this possibility, but the results indicate that if this intermediate exists, it is going to be kinetically insignificant.

b. Phosphate Hydrolysis. After release of the nucleoside a water molecule is proposed to hydrolyze the phosphate, upon which the $O_{Asp41}-P$ bond formed in the previous step breaks (Scheme 2). We replaced the dissociated nucleoside by a water molecule and reoptimized the structure. Now the $O_{water}-P$ distance (R2) is ca. 5 Å. For this step we choose R2 as the reaction coordinate. We shortened this distance in steps and optimized all other degrees of freedom. The results of this linear transit scan are shown in Figure 5.

As the lytic water approaches the phosphate it gradually loses its proton to the carboxylate group of Asp43 (R4 decreases), which now acts as a base. At the same time the $P-O_{Asp41}$ bond breaks gradually (i.e., R1 increases). From Figure 5 we notice that the hysteresis tendencies are much smaller for this step compared to the previous step. The curve is quite smooth around the highest point, which is found for R2 = 2.2 Å. At that distance the $O_{Asp41}-P$ bond (R1) is elongated from 1.86 to 2.13 Å and the proton of the lytic water is almost entirely transferred to Aps43 ($O_{water}-H$ = 1.37 Å and $H-O_{Asp43}$ = 1.11 Å). The highest energy found according to this stepping procedure is +14.3 kcal/mol in the gas phase and +22.3 kcal/mol with ϵ = 80.

Also, for this reaction step we managed to locate the exact unconstrained transition state (optimized structure shown in Figure 6). The R1 and R2 distances are 1.91 and 2.78 Å, respectively, i.e., very close to the corresponding values for the previous step (1.94 and 2.75 Å). In fact, the only difference between the two transition states is the substitution at the leaving group. The methyl of the leaving group in TS1 is now changed to a proton in TS2.

The energy barrier is calculated to be 6.8 kcal/mol in the gas phase and 12.6 kcal/mol using $\epsilon = 4$, values that are considerably lower than the linear transit results. The hydrolysis reaction step is calculated to be exothermic by 1.7 kcal/mol in the gas phase but becomes 7.1 kcal/mol endothermic after inclusion of solvation ($\epsilon = 4$).

As for the dissociation step, we tried but failed to locate a pentacoordinated intermediate for the hydrolysis step like the one shown in Scheme 2. Such an intermediate would correspond to a two-step hydrolysis reaction, where the proton of the lytic water is transferred to the Asp43 and the pentacoordinated intermediate is created, followed by a $P-O_{Asp41}$ bond-breaking step. The results of our calculations indicate, again, that if such an intermediate exists, it is quite insignificant from a kinetic point of view.

V. Conclusions

In the present paper we used large quantum cluster models to investigate reactions of deoxynucleotidase. The models were based on the X-ray structure of Rinaldo-Matthis et al.[6] and consist of up to 99 atoms.

The calculated energies provide quite strong evidence for the mechanism suggested by Rinaldo-Matthis et al.[6] In the first step the Mg−ligand Asp41 attacks the phosphate concerted with protonation of the leaving group by Asp43, which acts as an acid. In this dephosphorylation step no pentacoordinated intermediate could be located; inversion of the phosphate occurs simultaneously with the proton transfer from Asp43 to the leaving nucleoside. In the second half-reaction the hydrolysis of the phosphate Asp43 acts as a base, receiving a proton from the lytic water as it approaches the phosphate. No pentacoordinated intermediate could be located for this step either. The

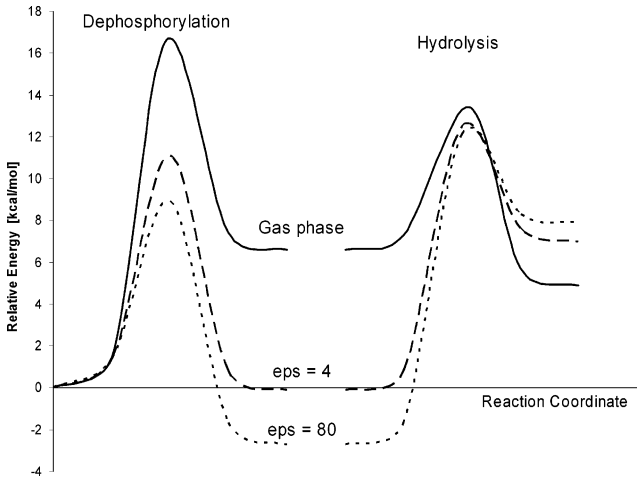

Figure 7. Calculated potential-energy curves for the dephosphorylation and hydrolysis steps studied in the present investigation.

calculated energetics are summarized in Figure 7 in the form of potential-energy curves. In the gas-phase calculations we note that the dephosphorylation is step is rate limiting, having a barrier of 16.6 kcal/mol compared to an accumulated barrier of 13.4 kcal/mol for the hydrolysis step. As we added the solvent effects (in the form of homogeneous continuum) the order was reversed. Using $\epsilon = 4$ the barriers are 11.1 and 12.5 kcal/mol for the first and second steps, respectively, and using $\epsilon = 80$ the corresponding values are 8.9 and 17.5, respectively. This different behavior between gas-phase and solvent energies is a result of the lack of explicit solvation of the Asp43 residue in our calculations.

Acknowledgment. The Wenner-Gren Foundation is acknowledged for financial support. We also thank the NSC for computer time.

References and Notes

(1) Reichard, P. *Annu. Rev. Biochem.* **1988**, *57*, 349.

(2) Rampazzo, C.; Johansson, M.; Gallinaro, L.; Ferraro, P.; Hellman, U.; Karlsson, A.; Reichard, P.; Bianchi, V. *J. Biol. Chem.* **2000**, *275*, 5409.

(3) Rampazzo, C.; Gallinaro, L.; Milanesi, E.; Frigimelica, E.; Reichard, P.; Bianchi, V. *Proc. Natl. Acad. Sci. U.S.A.* **2000**, *97*, 8239.

(4) Balzarini, J.; Aquaro, S.; Knispel, T.; Rampazzo, C.; Bianchi, V.; Perno, C. F.; De Clercq, E.; Meier, C. *Mol. Pharmacol.* **2000**, *58*, 928.

(5) Balzarini, J.; Naesens, L.; Aquaro, S.; Knispel, T.; Perno, C.; De Clercq, E.; Meier, C. *Mol. Pharmacol.* **1999**, *56*, 1354.

(6) Rinaldo-Matthis, A.; Rampazzo, C.; Reichard, P.; Bianchi, V.; Nordlund, P. *Nat. Struct. Biol.* **2002**, *9*, 779.

(7) Wang, W.; Kim, R.; Jancarik, J.; Yokota, H.; Kim, S. H. *Structure (Cambridge)* **2001**, *9*, 65.

(8) Hisano, T.; Hata, Y.; Fujii, T.; Liu, J. Q.; Kurihara, T.; Esaki, N.; Soda, K. *J. Biol. Chem.* **1996**, *271*, 20322.

(9) Toyoshima, C.; Nakasako, M.; Nomura, H.; Ogawa, H. *Nature* **2000**, *405*, 647.

(10) Lahiri, S. D.; Zhang, G. F.; Dunaway-Mariano, D.; Allen, K. N. *Science* **2003**, *299*, 2067.

(11) Allegrini, S.; Scaloni, A.; Ferrara, L.; Pesi, R.; Pinna, P.; Sgarrella, F.; Camici, M.; Eriksson, S.; Tozzi, M. G. *J. Biol. Chem.* **2001**, *276*, 33526.

(12) Rinaldo-Matthis, A.; Rampazzo, C.; Balzarini, J.; Reichard, P.; Bianchi, V.; Nordlund, P. *Mol. Pharmacol.* **2004**, *65*, 860.

(13) Lahiri, S. D.; Zhang, G. F.; Radstrom, P.; Dunaway-Mariano, D.; Allen, K. N. *Acta Crystallogr., Sect. D: Biol. Cryst.* **2002**, *58*, 324.

(14) a) Becke, A. D. *Phys. Rev.* **1988**, *A38*, 3098. (b) Becke, A. D. *J. Chem. Phys.* **1992**, *96*, 2155. (c) Becke, A. D. *J. Chem. Phys.* **1992**, *97*, 9173. (d) Becke, A. D. *J. Chem. Phys.* **1993**, *98*, 5648.

(15) Frisch, M. J.; et al. *Gaussian 98*, Revision A.11.4; Gaussian Inc.: Pittsburgh, PA, 2002.

(16) a) Klamt, A.; Schürmann, G. *J. Chem. Soc., Perkin Trans.* **1993**, *2*, 799. (b) Andzelm, J.; Kölmel, C.; Klamt, A. *J. Chem. Phys.* **1995**, *103*, 9312. (c) Barone, V.; Cossi, M. *J. Phys. Chem.* **1998**, *102*, 1995. (d) Barone, B.; Cossi, M.; Tomasi, J. *J. Comput. Chem.* **1998**, *19*, 404. (e) Cossi, M.; Rega, N.; Scalmani, G.; Barone, V. *J. Comput. Chem.* **2003**, *24*, 669.

(17) Frisch, M. J.; et al.*Gaussian 03*, Revision B.03; Gaussian Inc.: Pittsburgh, PA, 2003.